

Modelling Propagation in Multi-Floor Buildings using the FDTD Method

Andrew C. M. Austin, *Student Member, IEEE*, Michael J. Neve, *Member, IEEE*, and Gerard B. Rowe, *Member, IEEE*

Abstract— A three-dimensional parallel implementation of the FDTD method has been used to identify and isolate the dominant propagation mechanisms in a multi-storey building at 1.0 GHz. A novel method to visualise energy flow by computing streamlines of the Poynting vector has been developed and used to determine the dominant propagation mechanisms within the building. It is found that the propagation mechanisms depend on the level of internal clutter modelled. Including metallic and lossy dielectric clutter in the environment increases attenuation on some propagation paths, thereby altering the dominant mechanisms observed. This causes increases in the sector-averaged path-loss and changes the distance-dependency exponents across a floor from 2.2 to 2.7. The clutter also reduces Rician K -factors across the floor. Directly comparing sector-averaged path-loss from the FDTD simulations with experimental measurements shows an RMS error of 14.4 dB when clutter is ignored. However, this is reduced to 10.5 dB when the clutter is included, suggesting that the effects of clutter should not be neglected when modelling propagation indoors.

Index Terms— Finite difference methods, indoor radio communication, modeling, numerical analysis.

I. INTRODUCTION

THE increasing demand for wireless communication services has necessitated the reuse of frequency spectrum. Frequency reuse causes co-channel interference, which is detrimental to system performance, reducing the coverage area, reliability, throughput and the number of users that can be supported [1]. Characterising and mitigating co-channel interference in unlicensed bands remains a major challenge. Indoor systems are particularly susceptible as all transceivers are usually located in close physical proximity. Accurately predicting system performance depends heavily on correctly characterising the indoor propagation environment and a number of models to accurately and reliably predict signal strengths inside buildings have been proposed. Empirical models based on experimental measurements are often used, as the large variability in architectural styles and building materials can complicate deterministic modelling.

Empirical models typically use an exponential distance dependency to predict local means as a function of distance from the transmitter [2], [3]. Shadowing and fading are accounted for by including statistical variation around the local mean prediction [1]. However, empirically-based models cannot explain the physical observations and are thus hard to generalise.

Manuscript received January 1, 1900; revised January 2, 1900; accepted January 3, 1900. Colour versions of the figures are available online.

The authors are with the Department of Electrical and Computer Engineering at The University of Auckland, Auckland, New Zealand; email: acm.austin@ieee.org

For example, many of the terms and parameters in these models lack an electromagnetic basis, and vary considerably between buildings [1], [2]. Consequently, the applicability of empirical models in buildings where measurements were not taken remains a concern. When used in practice, empirical models have been found to result in pessimistic estimates of system performance [1]. More accurate findings have been reported when the empirical models were complemented with physical factors, such as correlated shadowing [1].

Site-specific ray-tracing methods—such as Geometrical Optics (GO) and the Uniform Theory of Diffraction (UTD)—have also been widely applied to model propagation within buildings [4]. However, ray methods must be applied to the indoor propagation problem with caution, as many of the assumptions and approximations used in their derivation are not valid for typical indoor environments. For example, structural corners made from lossy dielectric materials (such as concrete) are frequently encountered in indoor environments, however dielectric wedge diffraction is known to be a non-ray-optical process [5]. Correctly predicting the diffracted fields is important, as in some circumstances (e.g. deeply shadowed regions) the received power is dominated by diffracted components [6].

The relatively compact size of the indoor propagation problem, and advances in computational technology, are allowing the application of grid-based numerical techniques, such as the Finite-Difference Time-Domain (FDTD) method. Unlike ray-based methods, the FDTD technique does not make *a priori* assumptions about the propagation processes. Due to the high computational requirements of the FDTD method, previous studies have limited analysis to propagation on two-dimensional TM_z or TE_z horizontal ‘slices’ through the geometry [6]–[11]. However, two-dimensional results on a horizontal slice may fail to capture propagation mechanisms caused by interactions with the floor or ceiling and cannot be directly verified against experimental measurements. In practical indoor wireless communication systems, frequency channels are often reused between floors in a building, so characterising inter-floor propagation is important to predict the levels of co-channel interference [1]. It is important to note that, unlike the single-floor case, no single two-dimensional slice through a multi-floor geometry can correctly account for all possible propagation paths. For example, many buildings have concrete shafts containing elevators and stairwells, and propagation to adjacent floors around (or through) such shafts can only be thoroughly examined in three-dimensions. For this reason, we regard a three-dimensional characterisation of

fundamental importance.

Although a three-dimensional characterisation of the propagating fields using the FDTD method is useful, it is the identification and isolation of the dominant propagation mechanisms that is arguably more important—especially for system planners [12]. Specifically, the FDTD simulations can be used to determine which components are important to predict the sector-averaged mean, and which can be reliably ignored. One of the original contributions of this work is the identification (via a rigorous FDTD analysis) of the dominant propagation mechanisms, which could be incorporated into the development of accurate, yet efficient models, suitable for use by system planners on a day-to-day basis. In particular, this paper focuses on providing an independent deterministic validation of the Seidel model [2], and is underpinned with experimental measurements. (This is consistent with the philosophy adopted by Walfisch and Bertoni—in their characterisation of macro-cellular systems—who were able to deterministically explain (using Fresnel-Kirchhoff diffraction theory) the $\frac{1}{d^4}$ distance dependency of received power [13], which until then only had an experimental basis [14]).

A further contribution of this paper is an assessment of the impact of clutter in the environment (such as office furniture) on the dominant propagation mechanisms. Interestingly, most existing applications of time-domain methods to model propagation within buildings have assumed these buildings to be empty [6]–[11], [15]–[17] (though [11], [16], [17] did assess the impact of different wall types). However, actual office buildings contain varying amounts of furniture and other metallic and dielectric clutter. In this paper comparisons are made between a basic FDTD model (with a similar level of detail to models in the existing literature) and a more detailed model that includes some furniture and similar objects. Unlike many previous FDTD characterisations of the indoor radio channel, the findings reported in this paper are validated against independent experimental measurements of the path-loss and fading distributions.

A description of the FDTD models is presented in Section II. Section III describes a method of visualising the energy flow by tracing streamlines through the Poynting vector. Section IV presents the simulation results for propagation to the same and adjacent floors. Section V proposes models for the sector-averaged path-loss, while Section VI focuses on the statistical distributions characterising multipath fading. Also considered in Sections IV–VI are the effects of increasing the level of detail in the simulation models and comparisons against experimental measurements. Section VII briefly summarises the findings.

II. PROPAGATION MODELLING WITH THE FDTD METHOD

The building under investigation is the Engineering Tower at The University of Auckland. This is a typical eight-floor 1960's concrete slab building with a services shaft (containing elevators and stairwell) in the centre; in this paper three floors have been considered. The nominal values for the material properties used in FDTD simulation models are: Concrete: $\epsilon_r = 4.0$, $\sigma = 50$ mS/m; Glass: $\epsilon_r = 3.0$, $\sigma = 2.0$ mS/m;

Drywall: $\epsilon_r = 2.0$, $\sigma = 2.0$ mS/m; Wood: $\epsilon_r = 3.0$, $\sigma = 10$ mS/m; and metal: $\epsilon_r = 1$, $\sigma = 10^7$ S/m. The effects of internal detail/clutter are examined by considering two interior geometries, hereafter referred to as *basic* and *detailed*. The 0.20 m thick concrete floors, 1 cm thick exterior glass and the hollow concrete services shaft are common to both models.

The basic geometry adds internal walls (modelled as 4 cm solid slabs of drywall) creating a corridor around the shaft and dividing the remaining space into nine offices. The detailed geometry models the internal walls as two 1 cm sheets of drywall (separated by a 4 cm air-gap) attached to wooden frames with studs spaced 1.5 m apart. Against each wall, metal bookcases extend floor-ceiling—these contain books, modelled as 0.20 m thick wooden slabs. Doors into the offices and shaft are modelled as wood, and extend slightly into the corridor; the elevator doors are inset and modelled as metal. Metal reinforcing bars (2 cm square) are embedded in the concrete floors on a 1 m² grid, and metal window frames (2 cm square) are spaced 1.5 m apart on the external glass windows. Two flights of concrete stairs are also included in the central shaft.

A single E_z field component is excited with a modulated Gaussian pulse, given by $p(t) = \exp\left[-\left(\frac{t-t_0}{t_w}\right)^2\right] \sin(2\pi f_0 t)$ with parameters: $f_0 = 1.0$ GHz, $t_w = 1.25$ ns and $t_0 = 5t_w$. This produces a pulse with a 150 MHz 3-dB bandwidth centred around 1.0 GHz. The time step is 18.3 ps. A square lattice size of $\Delta = 1$ cm is used to minimise numerical dispersion [18, pp. 110–128]. The FDTD simulation domain is 18×18×9 m and is surrounded by a 12-cell thick convolutional perfectly matched layer (CPML) [18, pp. 294–310], resulting in approximately 3 billion mesh cells. Solving this problem using a single processor is not currently feasible and accordingly, the lattice is subdivided and allocated to multiple processors. Field values on the boundaries are exchanged every time step using an implementation of the Message Passing Interface [19]. On a 64-node computer cluster (using Intel Xeon 2.66 GHz processors) these problems require approximately 180 GB of memory and take 48 hours to solve to steady-state (15,000 time steps).

The steady-state electric and magnetic field magnitude and phase were extracted by multiplying the time-series with a 1.0 GHz cisoid. To compare the FDTD results against experimental measurements, the steady-state fields were converted to path-loss (in dB). The radiation pattern from a single E_z component is isotropic in the azimuth plane and proportional to $\sin \theta$ in the elevation plane (i.e. similar to a short dipole antenna). The steady-state E_z fields (in the radial direction) can be converted to path-loss by normalising the values to the Friis equation.

III. VISUALISING ENERGY FLOW

The time-averaged Poynting vector is given by

$$\mathbf{S} = \frac{1}{2} \Re[\mathbf{E} \times \mathbf{H}^*] \quad \text{Wm}^{-2}, \quad (1)$$

where \mathbf{E} and \mathbf{H} are the steady-state vector electric and magnetic fields respectively, and $*$ denotes the complex conjugate. At each point in the field, the Poynting vector indicates

the direction and magnitude of energy flow. Streamlines are projected through this space by applying principles developed in fluid dynamics for studying steady flows [20]. (A similar analysis using Poynting vector streamlines to visualise energy flow escaping backwards from a pyramidal horn antenna was reported in [21].)

The local tangent to a streamline is the vector representing energy flow at that point, and in three-dimensions the differential equation governing a streamline is given by

$$\frac{d\vec{p}(a)}{da} = \mathbf{S}(\vec{p}(a)), \quad (2)$$

where \vec{p} is the position, a is the parameter along the streamline, and $\mathbf{S}(\vec{p})$ is the Poynting vector at \vec{p} . Starting from an appropriate initial position, $\vec{p}(a)$, the streamline is computed by numerically solving (2) using forward differences (tracing the direction of the physical propagation of the Poynting vector out of the lattice) or backward differences (tracing the Poynting vector back to the transmitting antenna). The forward difference expression is given by

$$\frac{\vec{p}(a + \bar{a}) - \vec{p}(a)}{\bar{a}} = \mathbf{S}(\vec{p}(a)). \quad (3)$$

A step size $\bar{a} = 2\Delta$ (where Δ is the lattice cell size) was found to be a good trade off between computational efficiency and accuracy. In the case where $\mathbf{S}(\vec{p}(a + \bar{a}))$ does not lie on the down-sampled FDTD lattice, it is interpolated using values from adjacent cells. Linear interpolation was found to provide an adequate result. It should be noted that a single initial position results in one streamline which may not be representative of the dominant propagation mechanism in a region. To assist in the visualisation of the net energy flow in a region of space 100 points in a 3λ ‘cloud’ around the specified initial position are typically seeded.

IV. PROPAGATION MECHANISMS

A. Propagation on the Same Floor

Fig. 1(a) and (b) plot the path-loss on horizontal slices through the basic and detailed internal geometries. The slices are positioned 1.50 m from the floor, in the plane of the transmitting antenna (located at \times). Fig. 2(a) and (b) show streamlines (I–IV) of energy flow, calculated using (3) for both internal geometries. Initial points (\circ) were selected, such that streamlines I and III are shadowed by the central shaft, and II and IV are separated from the transmitter by soft partitions. The central services shaft is observed to significantly shadow waves propagating across the floor when the transmitters are diagonally positioned. Paths penetrating through the shaft are highly attenuated by the thick lossy concrete walls, and consequently, signals received in the shadowed regions are dominated by paths propagating around the shaft.

Energy reaching the shadowed regions in the basic geometry is observed to penetrate through the soft partitioned offices and reflects off the exterior glass windows. This is supported in both Fig. 1(a) and Fig. 2(a), where strong specular reflections from the glass are visible (e.g. streamlines I and II). The presence of strong reflected paths agrees well with previous two-dimensional FDTD simulations of empty buildings [6],

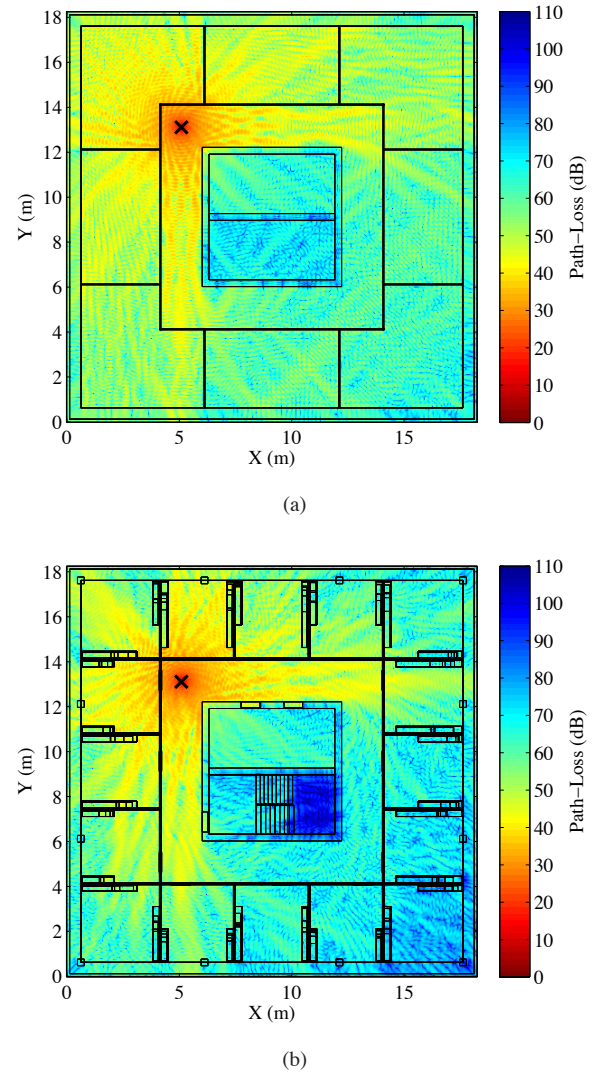
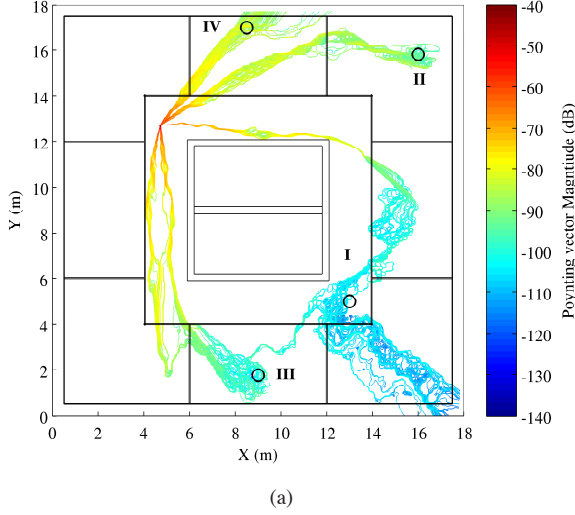


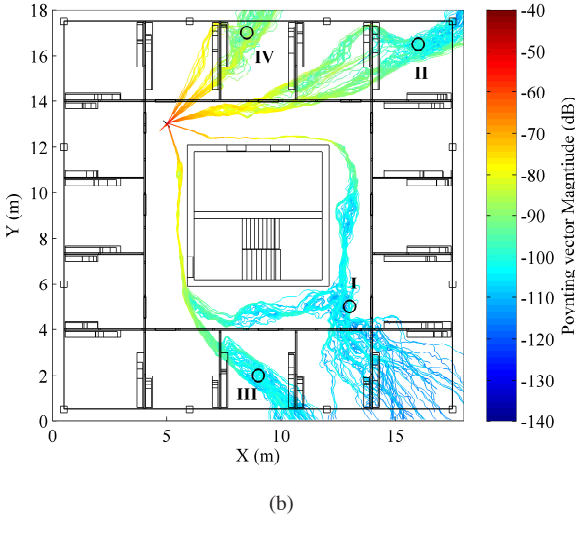
Fig. 1. FDTD simulated path-loss (at 1.0 GHz) on a horizontal slice through the first floor for: (a) basic internal geometry, and (b) detailed internal geometry. The location of the transmitter is indicated by \times , with the floor plan of the building superimposed.

[7], [10]. The problem is nominally symmetric and reflections from both sides of the building contribute equal amounts of power; the resulting $(3\lambda)^3$ sector-averaged path-loss in the shadowed regions is approximately 65 dB.

Comparing Fig. 1(a) with 1(b) and Fig. 2(a) with 2(b) shows a distinct change in the propagation mechanisms, namely strong reflected paths from the windows and drywall are no longer visible. When shelves and books are included against the internal walls, the reflected paths are attenuated to such an extent that (in this case) diffraction around the corners of the concrete shaft is observed to dominate propagation into the shadow regions. Paths involving diffraction exist in the basic geometry, but contribute a small proportion of the total received power. The inclusion of metal window frames also perturbs specular reflection from the glass. The sector averaged path-loss recorded in shadowed regions is up to 15 dB higher than the basic geometry. The attenuation introduced by a single layer of clutter in the environment only slightly reduces the



(a)

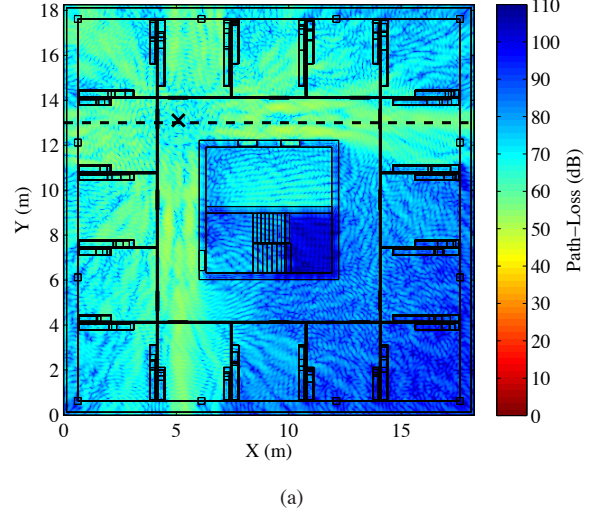


(b)

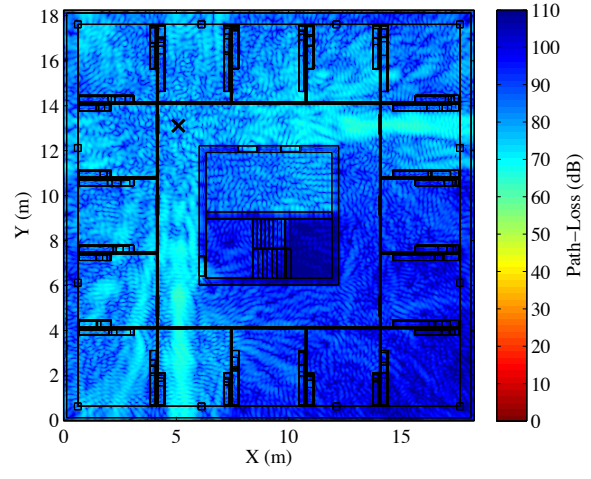
Fig. 2. Streamlines of energy flow through the single floor environment: (a) basic geometry and (b) detailed geometry. Seed points are marked with \circ . Four seed points (I–IV) are identified for each case.

received power. However, the accumulation of many such effects has the potential to cast significant radio shadows, and may result in other propagation mechanisms dominating. Clutter in the detailed geometry is also observed to introduce strong multi-path components when propagating through the walls, e.g. streamlines II and IV in Fig. 2(a) and (b). This behaviour also alters the fading distributions, and is discussed in further detail in Section VI.

For both the basic and detailed internal geometries, corridors have been modelled as largely clutter free. The sides of the corridor can be considered electrically smooth, and thus the corridor has potential to act as an over-moded waveguide. This mechanism has previously been observed experimentally for relatively long (> 30 m) corridors [22]. In our simulations, the 3λ sector average pathloss is observed to increase from 30 dB to 47 dB when moving 1.5–8.5 m away from the antenna, along the corridor. These values are between 3–5 dB lower than expected for free-space and are attributed



(a)



(b)

Fig. 3. FDTD simulated path-loss (detailed geometry at 1.0 GHz) for (a) one floor separating the transmitter and receiver, and (b) two floors separation. The location of the transmitter is indicated by \times .

to the reflections from the walls, ceiling and floor. At longer distances the angle of incidence becomes increasingly glancing and it is likely true waveguide modes may be formed.

B. Propagation to Adjacent Floors

Fig. 3 shows the path-loss on horizontal slices (a) one floor and (b) two floors above the transmitter for the detailed geometry (similar to Fig. 1, the slices are positioned 1.5 m above each floor). Comparing the distribution of path-loss one and two floors above the transmitter, Fig. 3(a) and (b), with the same floor case, Fig. 1(b), shows many similarities. In particular, the radio shadow cast by the shaft remains a dominant feature of the indoor environment, and propagation into the shadowed regions remains governed by diffraction at the corners of the shaft. Similar observations can be made for the basic geometry. Clutter in the environment is also observed to introduce strong local shadowing and multi-path. These results suggest that many of the mechanisms identified

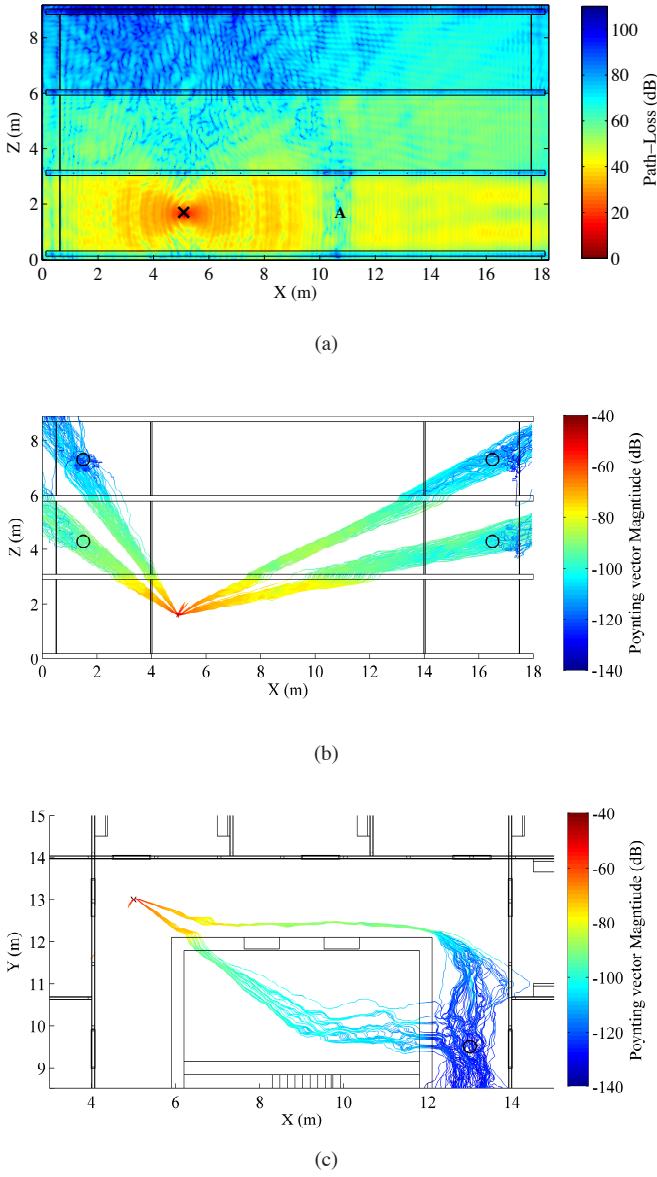


Fig. 4. (a) Vertical slice through the three-floor detailed geometry (along - - - indicated in Fig. 3(a)) (b) Poynting vector streamlines on the vertical slice for seed points located on the adjacent floors. (c) Streamline visualisations of propagation paths (from floor 1 to 3) that travel through the shaft.

in the same floor case still dominate propagation to adjacent floors. However, it is noted that the attenuation introduced by each floor is not constant and varies depending on the location of the receiver.

Fig. 4(a) shows the path-loss on a vertical ‘slice’ through the three-floor detailed geometry; the location of the slice is indicated by - - - in Fig. 3(a). The radiation pattern of the short dipole antenna (located at \times) causes greater path-loss in regions above the antenna. The lower path-loss around point ‘A’ can be attributed to reflection and scattering from the metal elevator doors. The metal rebar is observed to introduce local scattering, supporting the findings of [23], which showed greater multi-path is present when the rebar embedded in the concrete is included in the analysis. However, the dominant

propagation path—penetration through the concrete—remains largely unchanged. Fig. 4(b) shows streamline visualisations of the Poynting vector for four seed points (indicated by \circ , and centred on the vertical slice) located one and two floors above the transmitter. These streamlines largely follow line-of-sight (LOS) paths (though refraction is also visible at the air-concrete and concrete-air interfaces), indicating the dominant propagation mechanism (in this region) is penetration through the floors.

As more floors separate the transceivers, alternative propagation paths involving the lift-shafts and stairwells may contribute significant amounts of power, and may explain the variations in attenuation across each floor. Results indicate these paths are not dominant for a single floor separation. However, as indicated in Fig. 4(c), propagation into the lift-shaft can provide a comparable level of power two floors above the transmitter. (Streamline visualisations of the Poynting vector show the *net* energy flow, and for both paths to be present they have to contribute roughly equal power.) As the walls of the shaft are thicker than the floors, these paths are only visible after two floor penetrations. If the geometry was extended to four floors, paths propagating through the shaft would be expected to dominate the received signal. It should also be noted that, depending on the environment, propagation mechanisms external to the building perimeter may dominate the received power on other floors. Diffraction at a floor/window edge [24] and reflections from surrounding buildings [15] are two such examples.

V. PATH-LOSS PREDICTION MODELS

Fig. 5 shows scatter plots of $(3\lambda)^3$ sector-averaged path-loss (in dB) versus the transmitter-receiver separation distance. Only E_z field points from material-free regions are included in the sector-average. Higher path losses are observed in the detailed geometry, particularly on longer paths. Based on the results presented in Section IV, the change in propagation mechanism from reflection at the glass windows to diffraction at the concrete corner is responsible for the increased path-loss. Also evident in Fig. 5 are a number of sectors (in both geometries) with distance dependency exponents $n < 2.0$. These sectors occur in the corridors and are caused by strong reflections from the walls, ceiling and floor. Similar observations have been made in [7].

Similar to [2] models in the form d^n are used to relate the average path-loss with the transmitter-receiver separation distance

$$PL(d) = PL(d_0) + 10 \times n_{sf} \times \log_{10} \left(\frac{d}{d_0} \right) + \sum_{f=1}^F FAF_f \quad (\text{dB}), \quad (4)$$

where n_{sf} is the distance dependency exponent for data collected on the same floor as the transmitter, $PL(d_0)$ is the path-loss at reference distance $d_0 = 1.0$ m, d is the transmitter-receiver separation distance, FAF_f is the floor attenuation encountered propagating through the f^{th} floor, and F is the number of floor separations considered. The parameters n and FAF_f are found by fitting (4) to the data via linear regression, given $PL(d_0 = 1 \text{ m}) = 32.4 \text{ dB}$.

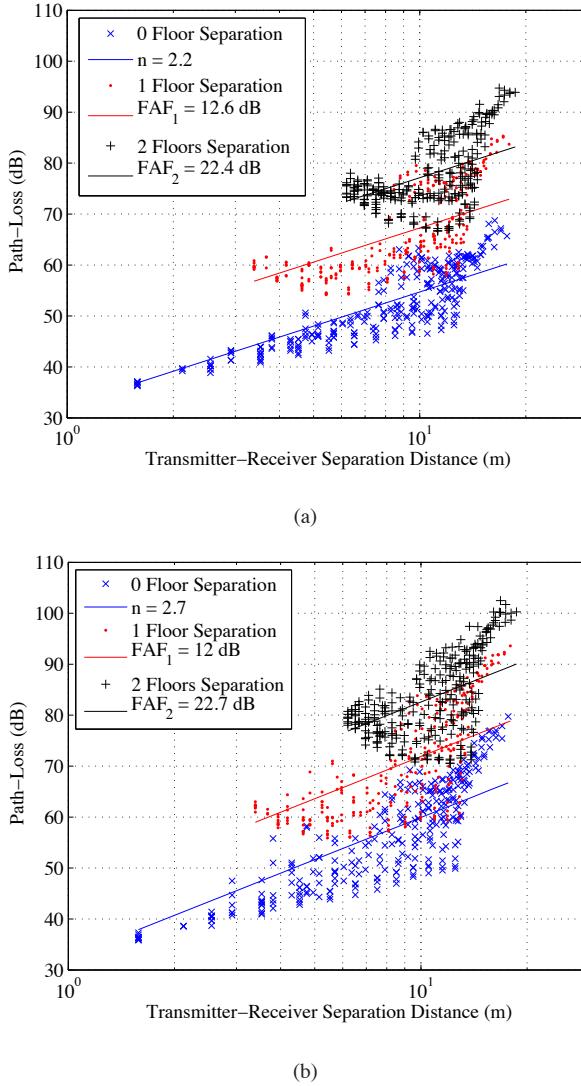


Fig. 5. Scatter plots of $(3\lambda)^3$ path-loss versus distance for (a) basic and (b) detailed internal geometries. The solid lines represent a Seidel model [2] fitted to the simulated data.

TABLE I
PARAMETERS FOR THE SEIDEL MODEL [2].

	Basic Geometry	Detailed Geometry	Exper. Meas.
All Regions	n_{sf}	2.2	3.6
	FAF ₁ (dB)	12.6	11.8
	FAF ₂ (dB)	9.8	11.0
	RMS error (dB)	5.3	7.4
Lit Regions	n_{lit}	1.9	2.9
	FAF ₁ (dB)	11.8	14.6
	FAF ₂ (dB)	11.0	14.2
	RMS error (dB)	3.0	6.1
Shadowed Regions	$n_{shadowed}$	2.6	4.2
	FAF ₁ (dB)	15.3	9.0
	FAF ₂ (dB)	8.3	6.6
	RMS error (dB)	3.6	4.8

Table I shows the least-squares best-fit distance dependency exponents, floor attenuation factors and RMS error between (4) and the FDTD and experimental data. The data collected across the floor has been divided into two regions, *lit* and *shadowed*, based on the position of the receiver relative to the transmitter and the concrete services shaft. When all regions are considered, the same floor distance dependency exponent increases for the detailed model due to increased attenuation through the clutter. The increase in RMS error for the detailed geometry also indicates scattering off the clutter introduces greater variability around (4). It is also observed that FAF₂ < FAF₁ for both geometries and the experimental measurements. If the only propagation path was through the floors, and if the floors were identical, FAF₁ = FAF₂, however, the observed decrease is between 1–3 dB. In other buildings, a greater decrease in the FAF is observed (e.g. FAF₁ = 12.9 dB and FAF₂ = 5.8 dB [2]), and this behaviour is difficult to explain experimentally [2].

As shown in Fig. 4(b), penetration through the floors is the dominant propagation mechanism in the lit regions (for both internal geometries), and consequently FAF₁ ≈ FAF₂. In the basic geometry $n_{lit} = 1.9$, which is close to free-space ($n = 2.0$). The streamline visualisations of the Poynting vector presented in section IV-A show the dominant propagation path in lit regions is largely LOS. The soft partitions do not perturb the propagating waves or introduce appreciable attenuation. However, in the detailed geometry $n_{lit} = 2.3$, which tends to indicate clutter in the environment introduces additional attenuation. This is also supported by examining streamlines II and IV in Fig. 2(b), which show the energy tends to propagate on non-LOS paths in the lit regions. The streamlines presented in Fig. 4(c) indicate other (lower-loss) propagation paths may dominate in the shadowed region. It is thought the presence of such paths is (partly) responsible for the decrease in FAF between one and two floor separations. It is noted that $n_{shadowed} > n_{lit}$ for both geometries and experimental measurements.

Comparisons with Experimental Measurements

To confirm the findings made with the FDTD method, experimental measurements were conducted at 1.8 GHz over two floors of the Engineering building. Similar to [1], the transmitter carrier frequencies were spaced 400 kHz apart allowing the power received from transmitters located on adjacent floors to be measured in a single sweep. Identical, vertically orientated, discone antennas were used in both transmitter and receiver, and located approximately 1.6 m from the floor. The radiation pattern of the discone antennas is isotropic in the azimuth plane and the gain was calculated from test measurements in an anechoic chamber. 52 measurements were made across the floor and the receiving antenna was rotated over a 1 m diameter locus to average out the effects of multipath fading. The voltage envelope was also recorded and used to determine the fading distributions.

As the relevant material properties do not change significantly over the 1.0–1.8 GHz frequency range [3], a direct comparison between the path-loss for 1.0 GHz FDTD simulations and 1.8 GHz experimental measurements only needs

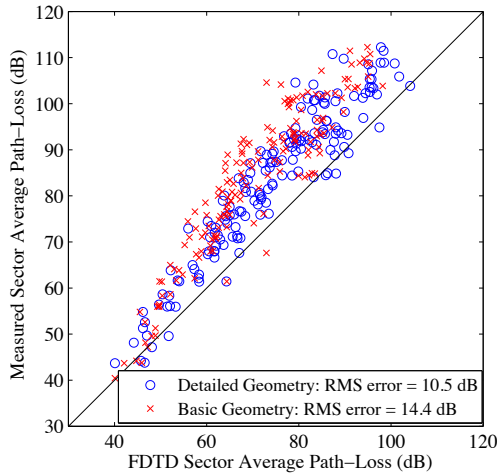


Fig. 6. Scatter plot comparing sector-averaged measurements of the path-loss with values obtained from FDTD simulations in the same locations. Both basic and detailed internal geometries have been considered, and in both cases the FDTD method generally underestimates the sector-averaged path-loss.

to account for the increased free-space loss (5.1 dB). Fig. 6 shows a point-wise comparison between the average path-loss recorded for the 104 experimental data points, and $(3\lambda)^3$ sector averaged FDTD simulations of the path-loss made at the same locations. It is noted that the FDTD simulations underestimate the path-loss for many sectors. This underestimation cannot be accounted for in the frequency difference; and is largest in regions furthest from the transmitter (and on highly cluttered paths) particularly paths shadowed by the shaft or passing through multiple partitions. Adding internal clutter improves the prediction accuracy, as shown in Fig. 6 the RMS error between the measurements and simulation is 14.4 dB for the basic geometry; this is reduced to 10.5 dB when the clutter is included. This result is significant, as it suggested that to correctly predict the path-loss, clutter present in the indoor propagation environment must be considered when applying full-wave electromagnetic methods. Although further environmental details/clutter could be added to improve the accuracy of the FDTD predictions, the random nature of the clutter (e.g. size, position and properties) complicates a fully-deterministic characterisation of the indoor radio channel.

VI. FADING DISTRIBUTIONS

Rayleigh and Rician distributions are frequently used to characterise multipath fading for indoor environments [1]. When a specular component is stronger than the scattered components—for example, on a line-of-sight (LOS) path—the probability density function (PDF) of the signal envelope follows a Rician distribution, given by

$$f(x) = \frac{x}{\sigma^2} \exp\left(\frac{-x^2 + s^2}{2\sigma^2}\right) I_0\left(\frac{xs}{\sigma^2}\right), \quad (5)$$

where s^2 is the power of the dominant component, $2\sigma^2$ is the mean scattered power, and I_0 is the zero-th order Bessel function of the first kind. The Rician K -factor is defined as

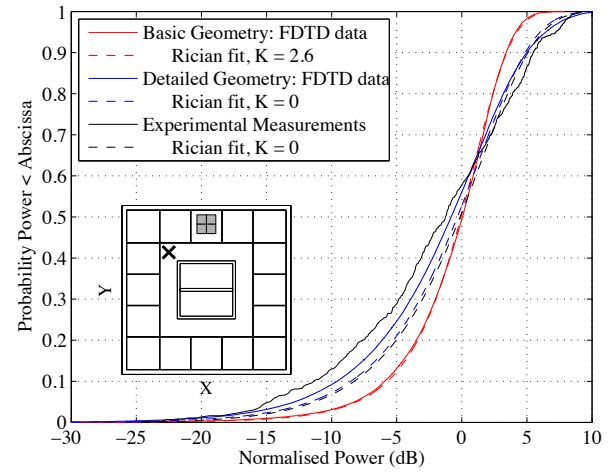


Fig. 7. Cumulative distribution functions of the received power envelope (in dB) normalised to the path-loss for both internal geometries and experimental measurements compared with exact Rician distributions. The E_z field data was recorded in the shaded regions on the same floor as the transmitter (located at \times).

the ratio of specular power to scattered power, $K = \frac{s^2}{2\sigma^2}$, and is determined from the FDTD simulated data using [25]

$$\frac{\mathbb{E}[x]}{\sqrt{\mathbb{E}[x^2]}} = \sqrt{\frac{\pi}{4(K+1)}} \exp\left(-\frac{K}{2}\right) \times \left[(1+K)I_0\left(\frac{K}{2}\right) + KI_1\left(\frac{K}{2}\right)\right], \quad (6)$$

where $\mathbb{E}[x^2]$ is the average square amplitude, $\mathbb{E}[x]$ is the average amplitude, and I_m is the m -th order Bessel function of the first kind. In the case where no single component dominates ($K = 0$), the PDF of the signal envelope follows a Rayleigh distribution, given by

$$f(x) = \frac{x}{\sigma^2} \exp\left(\frac{-x^2}{2\sigma^2}\right), \quad (7)$$

where σ^2 is the mean power.

Fig. 7 shows cumulative distribution functions (CDF) of received signal envelope (in dB) normalised to the mean path-loss for both internal geometries and experimental measurements. Also shown in Fig. 7 is a floor plan; the data was collected in the shaded sectors—located within an office, approximately 5 m from the transmitter. Rician distributions are fitted to these data sets using (6). In the basic geometry K is 2.6—this indicates a strong dominant component exists—whereas, in the detailed geometry and measurements $K = 0$, suggesting more energy is being scattered in this case. The experimental data set consists of 400 points, whereas the simulated data set has 2.5×10^5 points. Consequently, there is a greater variability between the experimental and theoretical CDFs, particularly at lower signal powers.

The differences in Rician K -factor for the basic and detailed geometries can be explained by examining streamline visualisations of the Poynting vector. Fig. 8 shows streamlines for the (a) basic; and (b) detailed geometries, reaching the same sectors considered in Fig. 7. In the basic geometry it is

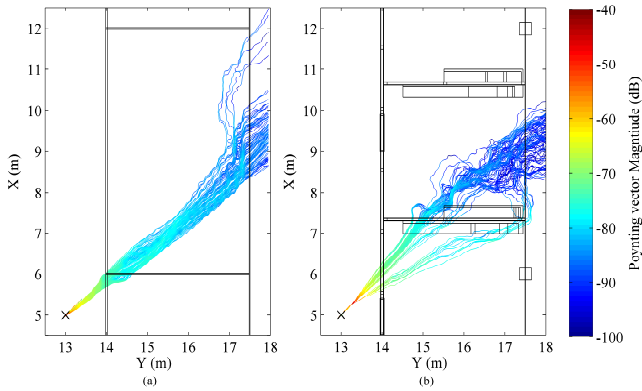


Fig. 8. Streamline visualisations of the Poynting vector traced from seed points (located in the shaded region in Fig. 7) to the transmitting antenna for (a) basic and (b) detailed internal geometries.

observed that the energy is travelling on the LOS path with some attenuation when penetrating through the soft partitions; accordingly, K is greater than zero. The same streamline in the detailed geometry shows the LOS path is blocked by bookshelves. The increased attenuation allows additional scattered paths (of similar magnitude to the attenuated-LOS path) to exist and accordingly, the PDF of the signal envelop follows a Rayleigh distribution. Similar phenomena are observed in other locations shadowed by clutter.

VII. CONCLUSIONS

A three-dimensional parallel FDTD algorithm has been used to identify and isolate the dominant propagation mechanisms in a multi-storey building. A simplified model based on the dominant mechanisms has been compared against experimental measurements of the path-loss. Streamline projections through the Poynting vector show that the dominant propagation mechanisms can change significantly when metallic and lossy dielectric clutter is included (the clutter also reduces Rician K -factors across the floor). The change in propagation mechanisms results in a lower RMS error when the FDTD simulation results are compared with measurements.

ACKNOWLEDGEMENTS

The authors wish to thank the reviewers for their valuable and useful comments; Ying Yang for her assistance with the experimental measurements; Yuriy Halytskyy and the Centre for eResearch at The University of Auckland for facilitating access to the BeSTGRID Auckland Cluster; and the New Zealand Tertiary Education Commission for providing a scholarship to A. Austin.

REFERENCES

- [1] K. S. Butterworth, K. W. Sowerby, and A. G. Williamson, "Base station placement for in-building mobile communication systems to yield high capacity and efficiency," *IEEE Trans. Commun.*, vol. 48, no. 4, pp. 658–669, April 2000.
- [2] S. Y. Seidel and T. S. Rappaport, "914 MHz path loss prediction models for indoor wireless communications in multifloored buildings," *IEEE Trans. Antennas Propag.*, vol. 40, no. 2, pp. 207–217, Feb. 1992.
- [3] Recom. ITU-R P.1238-6, "Propagation data and prediction methods for the planning of indoor radiocommunication systems and radio local area networks in the frequency range 900 MHz to 100 GHz," 2009.
- [4] S. Loredo, L. Valle, and R. P. Torres, "Accuracy analysis of GO/UTD radio-channel modeling in indoor scenarios at 1.8 and 2.5 GHz," *IEEE Antennas Propag. Mag.*, vol. 43, no. 5, pp. 37–51, 2001.
- [5] H. El-Sallabi and P. Vainikainen, "Improvements to diffraction coefficient for non-perfectly conducting wedges," *IEEE Trans. Antennas Propag.*, vol. 53, no. 9, pp. 3105–3109, 2005.
- [6] E. C. K. Lai, M. J. Neve, and A. G. Williamson, "Identification of dominant propagation mechanisms around corners in a single-floor office building," in *Proc. IEEE APS/URSI Int. Symp.*, 2008, pp. 424–427.
- [7] A. Alighanbari and C. D. Sarris, "Rigorous and efficient time-domain modeling of electromagnetic wave propagation and fading statistics in indoor wireless channels," *IEEE Trans. Antennas Propag.*, vol. 55, no. 8, pp. 2373–2381, Aug. 2007.
- [8] ——, "Parallel time-domain full-wave analysis and system-level modeling of ultrawideband indoor communication systems," *IEEE Trans. Antennas Propag.*, vol. 57, no. 1, pp. 231–240, Jan. 2009.
- [9] T. M. Schäfer and W. Wiesbeck, "Simulation of radiowave propagation in hospitals based on FDTD and ray-optical methods," *IEEE Trans. Antennas Propag.*, vol. 53, no. 8, pp. 2381–2388, Aug. 2005.
- [10] T. T. Zygaridis, E. P. Kosmidou, K. P. Prokopidis, N. V. Kantartzis, C. S. Antonopoulos, K. I. Petras, and T. D. Tsiboukis, "Numerical modeling of an indoor wireless environment for the performance evaluation of WLAN systems," *IEEE Trans. Magn.*, vol. 42, no. 4, pp. 839–842, April 2006.
- [11] Z. Yun, M. F. Iskander, and Z. Zhang, "Complex-wall effect on propagation characteristics and MIMO capacities for an indoor wireless communication environment," *IEEE Trans. Antennas Propag.*, vol. 52, no. 4, pp. 914–922, April 2004.
- [12] M. J. Neve, K. W. Sowerby, A. G. Williamson, G. B. Rowe, J. C. Batchelor, and E. A. Parker, "Physical layer engineering for indoor wireless systems in the twenty-first century," in *Proc. Loughborough Antennas Propag. Conf.*, 2010.
- [13] J. Walfisch and H. L. Bertoni, "A theoretical model of UHF propagation in urban environments," *IEEE Trans. Antennas Propag.*, vol. 36, no. 12, pp. 1788–1796, Dec. 1988.
- [14] K. Allsebrook and J. D. Parsons, "Mobile radio propagation in British cities at frequencies in the VHF and UHF bands," *IEEE Trans. Veh. Technol.*, vol. 26, no. 4, pp. 313–323, Nov. 1977.
- [15] A. C. M. Austin, M. J. Neve, G. B. Rowe, and R. J. Pirkle, "Modeling the effects of nearby buildings on inter-floor radio-wave propagation," *IEEE Trans. Antennas Propag.*, vol. 57, no. 7, pp. 2155–2161, July 2009.
- [16] M. Thiel and K. Sarabandi, "3D-wave propagation analysis of indoor wireless channels utilizing hybrid methods," *IEEE Trans. Antennas Propag.*, vol. 57, no. 5, pp. 1539–1546, 2009.
- [17] M. L. Stowell, B. J. Fasenfest, and D. A. White, "Investigation of radar propagation in buildings: A 10-billion element cartesian-mesh FETD simulation," *IEEE Trans. Antennas Propag.*, vol. 56, no. 8, pp. 2241–2250, Aug. 2008.
- [18] A. Taflove and S. C. Hagness, *Computational Electrodynamics: The Finite-Difference Time-Domain Method*, 3rd ed. Boston: Artech House, 2005.
- [19] "MPICH2: High-performance and widely portable MPI," March 2010, <http://www.mcs.anl.gov/research/projects/mpich2/>.
- [20] H. Landstorfer, H. Liska, H. Meinke, and B. Müller, "Energieströmung in elektromagnetischen wellenfeldern," *Nachrichtentechnische Zeitschrift*, vol. 25, no. 5, pp. 225–231, 1972, (in German). English Translation: "Energy Flow in Electromagnetic Wave Fields," *NASA Technical Translation*, NASA TT F-15,955. Oct. 1974.
- [21] J. F. Nye, G. Hygate, and W. Laing, "Energy streamlines: A way of understanding how horns radiate backwards," *IEEE Trans. Antennas Propag.*, vol. 42, no. 9, pp. 1250–1256, Sep. 1994.
- [22] D. Porrat and D. C. Cox, "UHF propagation in indoor hallways," *IEEE Trans. Wireless Commun.*, vol. 3, no. 4, pp. 1188–1198, July 2004.
- [23] R. A. Dalke, C. L. Holloway, P. McKenna, M. Johansson, and A. S. Ali, "Effects of reinforced concrete structures on RF communications," *IEEE Trans. Electromagn. Compat.*, vol. 42, no. 4, pp. 486–496, Nov. 2000.
- [24] W. Honcharenko, H. L. Bertoni, and J. Dailing, "Mechanisms governing propagation between different floors in buildings," *IEEE Trans. Antennas Propag.*, vol. 41, no. 6, pp. 787–790, June 1993.
- [25] F. van der Wijk, A. Kegel, and R. Prasad, "Assessment of a pico-cellular system using propagation measurements at 1.9 GHz for indoor wireless communications," *IEEE Trans. Veh. Technol.*, vol. 44, no. 1, pp. 155–162, 1995.



Andrew C. M. Austin was born in Auckland, New Zealand, on August 1, 1985. He received the B.E.(Hons.) degree in Electrical and Electronic Engineering from the University of Auckland, in 2007, where he is currently working toward the Ph.D. degree.

His research interests are in the areas of radiowave propagation, mobile communications and computational electromagnetics.

Mr. Austin was awarded a New Zealand Tertiary Education Commission Bright Futures Top Achiever Doctoral Scholarship in 2007.



Michael J. Neve was born in Auckland, New Zealand, on October 29, 1966. He received the B.E. (Hons.) and the Ph.D. degrees in Electrical and Electronic Engineering from the University of Auckland, in 1988 and 1993, respectively.

From May 1993 to May 1994, he was Leverhulme Visiting Fellow at the University of Birmingham, U.K. During this time, he was involved with radiowave propagation research using scaled environmental models. From May 1994 to May 1996, he was a New Zealand Science and Technology

Postdoctoral Fellow within the Department of Electrical and Electronic Engineering, University of Auckland where, from May 1996 to December 2000, he was a part-time Lecturer/Senior Research Engineer, and is currently a Senior Lecturer in the Department of Electrical and Computer Engineering. In 2004 he was a Visiting Scientist at the CSIRO ICT Centre in Sydney, Australia. His present research interests include radiowave propagation modelling in cellular/microcellular/indoor environments, the interaction of electromagnetic fields with man-made structures, cellular system performance optimisation and antennas.

Dr. Neve was jointly awarded a 1992/1993 Inst. Elect. Eng. Electronics Letters Premium for two publications resulting from his doctoral research.



Gerard B. Rowe received the B.E., M.E., and Ph.D. degrees in Electrical and Electronic Engineering from the University of Auckland, Auckland, New Zealand, in 1978, 1980, and 1984 respectively.

He joined the Department of Electrical and Computer Engineering, University of Auckland, in 1984 where he is currently a Senior Lecturer. He is a member of the Departments Radio Systems Group and his (disciplinary) research interests lie in the areas of radio systems, electromagnetics and bioelectromagnetics. Over the last 20 years he has taught

at all levels and has developed a particular interest in curriculum and course design. Currently, his educational research activity is concentrated on the secondary-to-tertiary transition and on the development of course concept inventories.

Dr. Rowe is a member of the IET, the Institution of Professional Engineers of New Zealand (IPENZ), ASEE, STLHE, and AaeE. He was the joint recipient of the 1993 Inst. Elect. Eng. Electronics Letter Premium Award for the papers "Assessment of GTD for Mobile Radio Propagation Prediction" and "Estimation of Cellular Mobile Radio Planning Parameters Using a GTD-based Model" which he coauthored. He has received numerous teaching awards from his institution. In 2004 he was awarded a (National) Tertiary Teaching Excellence Award in the Sustained Excellence in Teaching category and in 2005 he received the Australasian Association for Engineering Education award for excellence in Engineering Education in the Teaching and Learning category.